The influence of microchemistry on the softening behaviour of two cold-rolled Al-Mn-Fe-Si alloys

Ke Huang[1]*, Ning Wang[1], Yanjun Li[1,2], Knut Marthinsen[1]

[1] Department of Materials Science and Engineering,

Norwegian University of Science and Technology (NTNU), Trondheim 7491, Norway

[2] SINTEF Materials and Chemistry, N-7465 Trondheim, Norway

Abstract: The influence of microchemistry on the softening behaviour of two cold-rolled Al-Mn-Fe-Si alloys with different initial amounts of Mn (0.4 and 1.0 wt%, respectively) is studied. In addition to their as-cast conditions, the supersaturated Al-Mn-Fe-Si alloys were appropriately homogenized at two different conditions, which together produce three different states of microchemistry for each alloy, i.e. solutes and second-phase particles. Samples with different microchemistry states were then cold-rolled before subsequent back-annealing at different temperatures for the two alloys. The softening and concurrent precipitation behaviours of the samples have been monitored by hardness and electrical conductivity measurements respectively, and the final microstructure in terms of grain structure and texture has been characterized by EBSD. It is clearly demonstrated that the amount of Mn and the actual microchemistry state as determined by the homogenization procedure strongly influence the softening behaviour. Both a fine dispersion of pre-existing dispersoids and strong concurrent precipitation may slow down the recrystallization kinetics considerably and give a very coarse grain structure and textures commonly associated with dispersoids effects, although some are slightly atypical.

Key words: Recrystallization; Homogenization; EBSD; recrystallization texture; dispersoids; concurrent precipitation; Aluminium alloy

* **Corresponding author**: Dr. Ke Huang, Department of Materials Science and Engineering, Norwegian University of Science and Engineering, Trondheim 7491, Norway. Email: ke.huang@ntnu.no,

Tel: +47 73594004, Fax: +47 73550203

1 Introduction

The final properties of rolled particle-containing AA3xxx Al alloy sheets result from a series of successive and concurrent metallurgical reactions taking place during thermo-mechanical processes. Tailor-made microstructures and hence mechanical properties can only be obtained when all the phenomena occurring during these thermo-mechanical processes are well understood.

It is well known that intermetallic particles are of the outmost importance in recrystallization of deformed aluminium alloys containing second-phase particles [1-7]. However, their various effects on microstructure and texture evolution during thermo-mechanical processing, strongly depend on their size and distribution. Small and numerous dispersoids (typically formed during homogenization and/or subsequent heat treatments) tend to hinder boundary motion and slow down recrystallization and grain growth through a Zener drag effect [8]. By contrast, coarse constituent particles, formed during casting, can accelerate recrystallization by particle stimulated nucleation (PSN) due to the large amount of stored energy that concentrate next to them during cold rolling [9].

Whether the small dispersoids are introduced during homogenization (pre-existing dispersoids) or subsequent annealing after deformation (concurrent precipitation) will have an influence on the softening behaviour. It is well documented that a suitable homogenization cycle may strongly facilitate the down-stream recrystallization of Al sheet [10-16]. The size and number density of pre-existing dispersoids can be altered by different homogenization conditions. Concurrent precipitation usually occurs on the prior boundaries and retards recrystallization, especially at low annealing temperatures [17]. Microstructure evolution during the homogenization heat treatment of Al-Mn-Fe-Si alloys has been investigated using a combination of numerical and experimental studies by Du et al [18]. Recrystallization texture

evolution has also been investigated extensively since it determines the plastic anisotropy of the material. Factors affecting texture evolution are complex, including initial textures [19], deformation history [20], annealing temperatures [21], and particle structures [2, 6, 22]. After annealing of cold rolled sheets, weak textures are usually observed due to nucleation by PSN. The P and ND-rotated cube texture components have been reported in highly supersaturated aluminium alloys after large reduction of cold rolling and annealing at low temperatures [8, 23-27]. However, despite a lot of work focused on these issues [17,27], the understanding of the interaction between particles and softening behaviour is still incomplete and adequate quantitative descriptions/models are limited. This is a general challenge for process optimization and alloy design for tailor made properties of these particle-containing alloys, especially for the recycled aluminium alloys where alloying elements like Mn, Fe, and Si are accumulated.

The objective of the current work is to elucidate the impact of microchemistry state, i.e. solutes and second-phase particles on the softening behaviour of cold rolled Al-Mn-Fe-Si alloys. Two model alloys with different initial amounts of Mn (0.4 and 1.0 wt%, respectively) were used in this study, different homogenization procedures were performed which gave different microchemistry states suitable for analysing the effects of pre-existing particles and concurrently precipitated ones. Samples with different microchemistry states were then cold-rolled before subsequent back-annealing at different temperatures for the two alloys. The softening and concurrent precipitation behaviours of the samples have been monitored by hardness and electrical conductivity measurements respectively at different conditions, and the final microstructure in terms of grain structure and texture has been characterized by EBSD. The present paper is part of a comprehensive investigation on particle-annealing interactions in AA3xxx alloys involving both industrial and academic partners, to obtain a better understanding of the evolution of microstructure and texture and their interactions with second-

phase particles during cold rolling and subsequent annealing of AA 3xxx type alloys [28-31], as basis for validation and further development of relevant microstructure models [e.g.32] accounting for these aspects.

2 Experimental

2.1 Alloy conditions and annealing treatment

The investigated alloys were commercial DC-cast AA3xxx extrusion billets of 288 mm in diameter, supplied by Hydro Aluminium, from which slabs were machined from the central region. The as-received materials for both model alloys were in as-cast state, with the chemical compositions given in Table 1..Both materials consist of grains of equiaxed shape with average grain size of ~140 μm, and constituent particles are mostly located at the grain boundaries and in interdendritic regions. These two model alloys are designated as C1 and C2 respectively, to make it consistent with other related investigations [30-34].

The received C1 and C2 materials were subsequently homogenized at two different conditions to get different microchemistries, *i.e.* solute level and second-phase particle. The homogenization treatments were performed in an air circulation furnace with a temperature accuracy of ± 2 K, starting from room temperature (about 20 °C). One set of the samples for both model alloys C1 and C2 were heated at 50°C/h to 450 °C and kept for 4 hours, referred to as C1-2 and C2-2, respectively. Another set of the samples were subjected to a two-stage homogenization treatment. The samples were first heated at 50°C/h to 600 °C for 4 hours, and then cooled at 25°C/h to 500°C where they were kept for another 4 hours, which gave the C1-3 and C2-3 conditions, respectively. Materials were water quenched to room temperature at the end of the homogenization procedure to freeze the state of supersaturation/precipitation.

The homogenized materials together with the materials of the as-cast condition, which are labelled as C1-0 and C2-0, were cold rolled at room temperature from slabs of a thickness of 30 mm to 1.5 mm in multiple passes, which gave a relatively large strain of $\varepsilon = 3.0$. Cold rolling was performed in a laboratory rolling mill at the Norwegian University of Science and Technology. The rolling were carried out using heavy lubricated rolls and maximum roll velocity in order to obtain a microstructure similar to industrially rolled materials. The rolled sheets were subsequently isothermally back-annealed in a pre-heated salt bath at temperatures in the range of 300-500 °C and with different holding times in the range of $5\text{-}10^5$ s, followed by quick water quenching.

2.2 Microstructure characterization

The softening and precipitation behaviours during annealing were followed by Vickers hardness (VHN) and electrical resistivity measurements performed on the RD-TD plane of the sheets. Each reported value was obtained by averaging eight measurements. Electrical conductivity was measured by a Sigmascope EX 8 instrument at room temperature of about 293 K (20°C). Metallographic examinations of constituent particles and dispersoids were done by backscattered electron channelling contrast imaging in a Zeiss Ultra 55 field emission gun scanning electron microscope (FEG-SEM). Images were captured electronically and analysed using standard image analysis software Image-J, by which the characteristic size parameters of constituent particles, equivalent diameter d and number density were measured. For the hardness measurements, a load of 1 Kg, a loading time of 15 s and a loading speed of $100\mu ms^{-1}$ were used.

The crystallographic textures of the sheets were measured by means of EBSD (Electron backscattered diffraction) in a Zeiss Supra/Ultra 55 SEM equipped with TSL software. Orientation maps of both deformed and annealed samples, covering typically more than one

thousand grains (except the cases with extremely large grains), with step size of 1-2 μm, were used to study the orientation of the recrystallized grains and thus the texture evolution during recrystallization.

For selected conditions, characterization by SEM/EBSD was carried out so that the effect of homogenization and level of Mn in solid solution on the softening behaviour in terms of microstructure and texture evolution of the different Al-Mn-Fe-Si alloys could be studied. For all of the micrographs presented in this paper, the horizontal direction corresponds to the rolling direction (RD) while the vertical direction is the normal direction (ND). The grain size was measured as the equivalent circular diameter in the RD-ND cross section. The texture was determined by single grain orientation measurements by EBSD. From the single grain orientation measurements the ODF was calculated. Since all of the interested recrystallization textures for the current study are located in the ODF section with $\varphi_2=0^o$, only this section is presented for each condition.

3 Results and discussion

3.1 Microstructure and microchemistry before back annealing

Examples of the typical microstructure of both the as-cast and deformed materials are shown below in Fig.1. In the as-cast state, the material has a characteristic of equiaxed grain structure with an average grain size of ~140 μm, as shown in Fig.1a. After deformation to a strain of ε = 3.0, the material shows a banded deformation structure with most of the high angle grain boundaries aligned with the rolling direction (Fig. 1b)

The morphology and distribution of constituent particles and dispersoids in the as-cast state and the two as-homogenized states are illustrated in Fig. 2 and the quantitative values of their number densities and sizes, as well as solute levels of Mn, are given in Table 2. The sizes and number densities of both the constituent particles and/or dispersoids for C2 are larger than that of C1 for all the corresponding three variants, while the electrical conductivity values are smaller, the latter reflecting the differences in solute level on Mn. The as-cast variants, C1-0 and C2-0, have no pre-existing dispersoids, but have higher potential for concurrent precipitation due to their higher concentration of Mn in solid solution. For the variants C1-2 and C2-2, a large number of fine dispersoids (shown as inset in Figs. 2b and e) can be observed. The dispersoids are larger in size for C1-3 and C2-3 but the number densities are lower than in the former variant. In all the homogenized variants the solute levels of Mn are significantly reduced as compared to the as-cast variants, significantly reducing the potential for concurrent precipitation for these conditions.

3.2 Softening and precipitation behaviour

The response to isothermal annealing treatments of the samples cold-rolled to $\varepsilon = 3.0$ after different homogenization procedures was studied by measurements of hardness as a function of annealing time at different temperatures as illustrated in Figs. 3a-c. At the lowest temperature of 300 ^{o}C, the decrease of hardness is very slow, mainly due to recovery, however for C1-3 and C2-3 fully recrystallized states are still obtained after long annealing times of 10^4 s and 10^5 s, respectively. On the other hand, for all the cases, both C1 and C2 were fully recrystallized within 5 s when annealing at 500 ^{o}C. Comparison of the hardness-time curves of the two alloys at 400 ^{o}C reveals that C1 exhibits a faster softening kinetics than C2 where the latter has a higher solute content of Mn and thus higher potential for concurrent precipitation during annealing. A higher initial amount of Mn content also affects the strength after complete

recrystallization, the hardness of C2 was higher than that of C1, which can be attributed to the combined effect of solid solution hardening and dispersion hardening by dispersoids in the former case. The softening behaviour was also affected by different homogenization treatments, with C1-0 and C2-0 showing the slowest kinetics while C1-3 and C2-3 exhibit the fastest softening behaviour at the same temperatures. C1-3 and C2-3, which were homogenized at a higher temperature, have a low level of solute and a coarser pre-existing dispersoid structure (see Table 2) and thus less concurrent precipitation, both of which lead to faster recrystallization kinetics as well as a lower hardness value for the fully recrystallized state.

As revealed in Figs. 3d-f, the electrical conductivity of the three variants of both C1 and C2, which are at their lowest values before annealing, increase in general with time as more and more Mn is precipitated from the supersaturated solid solution. C2 shows a more pronounced increase in EC than C1 for all the three variants, indicating that precipitation is weaker for C1, which is again due to the lower initial alloy content of Mn and hence a weaker potential for precipitation. Different homogenization conditions also affect the EC evolution, where it is evident that the EC of the as-cast variants increased more than that of the other two variants, suggesting more concurrent precipitation in these materials. It should be noted that the increase in EC was normally limited in the first 10 s, while recrystallization could be completed within this period for the cases annealed at higher temperatures. At the highest temperature of 500 ^{o}C, the increases of EC were less pronounced than for the cases of annealing at 400 ^{o}C, probably due to less/minor precipitation at the higher temperature.

3.3 Microstructure and texture

The microstructures and textures of the cold-rolled Al-Mn-Fe-Si alloys after annealing for 10^5 s at different temperatures are presented in Figs. 4-9 below. Comparing the recrystallized microstructures of the cold-rolled C1 and C2 alloys with different homogenization procedures,

it is found that both the homogenization procedure and solute level of Mn strongly affect the recrystallized grain structure and texture.

Annealing of cold-rolled C1-0 and C2-0 variants for 10^5 s at both 400 ^{o}C and 500 ^{o}C leads to fully recrystallized structures, as shown in Fig. 4. However, much smaller grain sizes are found for C1-0 than C2-0 after annealing at the same temperatures. As indicated by Fig. 3, the recrystallization process is strongly affected by concurrent precipitation at 400 ^{o}C both for C1-0 and C2-0, yielding large pan-cake shaped grains, especially for the C2 alloy for which the grains are very large. This is consistent with the larger amount of concurrently precipitated dispersoids in C2-0 (see Fig.3d), which provide a strong pinning effect on grain boundary migration. The significant difference in grain size also indicates that the presence of concurrent precipitation have had strong effect on suppressing the nucleation activity. This is an important observation as it clearly demonstrates that the nucleation kinetics is not truly site-saturated, an assumption often made for nucleation of recrystallization in aluminium alloys. Increasing the annealing temperature to 500 ^{o}C, where the interaction between concurrent precipitation and recrystallization was mostly avoided, recrystallization is completed within 5 s both for C1-0 and for C2-0, and a much refined grain structure was produced for both materials. Nonetheless, it is worth noticing that while a homogeneous microstructure with equiaxed grains was obtained for C1-0, the recrystallized grains for C2-0 are larger and still slightly elongated, indicating some effects of concurrent precipitation also at this temperature for this material.

When annealing the cold-rolled as-cast samples, the effects of dispersoids can only be attributed to the concurrent precipitation that took place during annealing. As illustrated in Fig. 5, the textures at these conditions are characterized by P and ND-rotated cube components, while a very weak RD-rotated cube component was also visible when annealing at 500 ^{o}C. For both C1-0 and C2-0, the intensities of the texture components generally decrease with

annealing temperature increasing from 400 ºC to 500 ºC, where for the latter case the recrystallization completes in 5s and interaction between recrystallization and concurrent precipitation was largely weakened or absent. As shown in Fig. 5b, the presence of a true cube texture component (quite weak) was only obtained for C1-0 at 500 ºC, where an equiaxed grain structure was obtained. On the other hand, for C2-0 annealed at 400 ºC, i.e. the case mostly affected by concurrent precipitation, a sharp 45º ND-rotated cube texture (indeed not a common texture component), together with a relatively weak P texture and 20 º ND-rotated cube texture (see Fig.5c), was obtained.

Different from the as-cast states, a large amount of fine dispersoids was already presented in the C1-2 and C2-2 conditions before annealing. Nonetheless, some additional concurrent precipitation also took place during annealing (most pronounced in C2-2; cf. Fig. 3e). Both of which affected the softening behaviour and thus the final microstructure, as demonstrated in Fig. 6. In all these cases with pre-existing dispersoids, the recrystallized grains were elongated along the rolling direction even though this elongation was less pronounced at the highest temperature of 500 ºC. Similar to annealing of the cold-rolled as-cast materials (see Fig.4), larger recrystallized grain sizes were obtained for C2-2 than that of C1-2 at the same temperatures. Besides, coarser recrystallized grain structures were also obtained at the lower annealing temperature of 400 ºC, both for C1-2 and C2-2 and most pronounced for the latter. The slow recrystallization kinetics and, consequently, the coarse grain structures obtained for C2-2 variant is a result of a combination of two effects: (i) a considerable amount of fine pre-existing dispersoids strongly affecting both nucleation and growth, (ii) a significant amount of additional concurrent precipitation as indicated by the EC evolution in Fig. 3e, especially at 400 ºC, and much stronger in C2-2 than C2-1. As compared to the as-cast variants shown in Fig. 4, both C1-2 and C2-2 have smaller grain sizes after annealing at 400 ºC, while larger grain sizes after annealing at 500 ºC than their as-cast counterparts. This is because, during

annealing at 500 ^{o}C, recrystallization has mostly completed in C1-0 and C2-0 before any substantial concurrent precipitation of dispersoids, while the pre-existing fine dispersoids in C1-2 and especially C2-2, will suppress partly the nucleation of recrystallization. During annealing at 400^{o}C, due to the slow recrystallization kinetics, a significant concurrent precipitation of fine dispersoids along subgrain boundaries and dislocations will happen in the as-cast variant before nucleation of recrystallization. These concurrently precipitated fine dispersoids have a stronger effect on retarding recrystallization than the pre-existing dispersoids in C1-2 and C2-2.

Medium strength textures were obtained for C1-2 and C2-2 after annealing at 400 ^{o}C and 500 ^{o}C, except for the case of C2-2 annealed at 400 ^{o}C where a very strong ND-rotated cube texture component and a relatively weak P component were found, as illustrated in Fig.7. The recrystallization textures of the two C1 variants, which both have less pre-existing dispersoids and less concurrent precipitation, are composed mainly of a Cube component with elements of ND-rotated cube combined and a weak P texture component. For the two C2 variants, on the other hand, the textures were dominated by a 35^{o} ND-rotated cube texture component together with the P texture component. The strength of the textures decreased for both C1-2 and C2-2 when the annealing temperature increased, however the texture components were almost the same.

For the variants homogenized at a higher temperature, *i.e.*, C1-3 and C2-3, characterized by a low solute level of Mn, and a coarse dispersoid structure, the retarding force from both pre-existing dispersoids and concurrent precipitation were weaker than that of the other homogenization variants as well as the non-homogenized conditions. This is clearly manifested in the markedly refined recrystallized grain structures for all the cases, as shown in Fig. 8. During annealing at 300 ^{o}C, C1-3 was fully recrystallized after 10^{4} s which was faster than its

counterpart C2-3. Moreover, a much finer recrystallized grain size was obtained for C1-3 after annealing at 300 ^{o}C, consistent with it being even less affected both by pre-existing dispersoids and concurrent precipitation than C2-3, which does contain some more pre-existing dispersoids (coarse though) and where some additional concurrent precipitation actually also seem to take place (cf. Fig. 3c). A characteristic feature of the C2-3 grain structure after annealing at 300 ^{o}C that is also worth noticing is the inhomogeneous structure in terms of grain size, implying concurrent precipitation of dispersoids has played a more significant role in retarding the nucleation of recrystallization at this condition. On the other hand, increasing the annealing temperature to 400 ^{o}C, resulted in a very fine grained and homogeneous structure, with a grain size slightly smaller than that of C1-3. This latter result can most probably be ascribed to enhanced nucleation by PSN, since the C2-3 material contains more constituent particles which is larger than the typical critical size for PSN nucleation (>1 μm).

From Fig. 9, it can be seen that a relatively strong cube texture component is obtained for both C1-3 and C2-3, together with a weak P component. The lowest cube texture intensity is obtained for C2-3 at 300 ^{o}C, however, weak P, RD-rotated and ND-rotated cube texture components are also present. Consistent with its coarser recrystallized grain structure shown in Fig.8c, the reason for this is most likely a combination of pre-existing dispersoids and a somewhat higher concurrent precipitation activity for this condition (cf. Fig 3f). For both C1-3 and C2-3, the intensities of the cube texture components increased when the annealing temperature increased from 300 ^{o}C to 400 ^{o}C.

The results presented in Figs. 3 -9 has clearly demonstrated that both small pre-existing dispersoids and concurrent precipitation in the alloys investigated may have a strong effect on both softening kinetics as well as recrystallized grain size and texture. The effects are dependent of the size and amount of dispersoids, and whether they exist before substantial

recrystallization process starts. A higher nominal content of Mn in the alloys will favour more pre-existing dispersoids after homogenization and more concurrent precipitation of dispersoids. However, with respect to possible differences between the two cases of pre-existing fine dispersoids or concurrent precipitation, the picture is not equally clear. Which one has stronger effect seems to be a subtle balance between alloy content, microchemistry state after homogenization and annealing conditions, whether concurrent precipitation interacts with recrystallization also matters. E.g. for the C1 alloy concurrent precipitation seems to be more influential, but only at the lowest annealing temperature of 400 ^{o}C (cf. Fig. 4a and Fig.6a), while for the C2 material annealed at 500 ^{o}C, pre-existing fine dispersoids seems to provide a larger effect (cf. Fig. 4d and Fig.6d) due to the fact that recrystallization completed within 5s and its interaction with concurrent precipitation was mostly avoided. Concerning recrystallization textures, concurrent precipitation seems to have more pronounced effect for C1, while for C2 both type of dispersoids effects (pre-existing or from concurrent precipitation) have a strong effect. These results are only partly consistent with the results of Tangen *et al* [27], who found that dispersoids present prior to cold rolling and annealing had a weaker effect on the recrystallized grain size and texture compared to concurrent precipitation. The effects of concurrent precipitation and pre-existing dispersoids are investigated further below with focus on conditions mainly controlled by the nucleation phase.

3.4 Effect of microchemistry state on nucleation of recrystallization

It is shown in the previous sections that both pre-existing particles and concurrent precipitation may strongly affect recrystallization kinetics, grain structure and texture. During

recrystallization at the highest temperature of 500 °C, recrystallization complete within 5 s and only limited concurrent precipitation occurs during this period of time (see Fig.3), except for the two as-cast variants where a slightly more distinct increase in EC is seen already at this early stages as compared to the homogenized variants. It opens for the possibility to analyse more closely how the microchemistry state and evolution affect the nucleation process.

The microstructures and textures of the three variants of the C1 alloy annealed at 500 °C for 5 s are shown in Fig.10 and Fig.11, respectively. As illustrated in Fig.10a, a structure of slightly elongated grains is obtained for C1-0, which indeed indicates that some concurrent precipitation actually has occurred. For the C1-2 variant the grains are larger than for C1-0, *i.e.* the nucleation density is lower, suggesting that the pre-existing dispersoids in this variant has acted to suppress nucleation, since the effect of concurrent precipitation is weaker than for C1-0. For C1-3, where the pre-existing dispersoid structure is coarser than that of C1-2, an equiaxed grain structure with the finest grain size is obtained, which further support the assumption that the pre-existing dispersoids in C1-2 do suppress nucleation. The reduced grain size for C1-3 may also partly be attributed to increased nucleation by PSN, however, the effect is expected to be weak since the size of constituent particles is only ~1 μm and the typical P texture component often accompanying with PSN is really weak in this case (Fig.11c). According to Fig. 11, the texture intensities generally increase from C1-0 to C1-3 with a distinct change in character. For C1-0, weak P and ND-rotated cube components, typical concurrent precipitation texture components, are dominating. The strength of these two components is fairly weak though, consistent with the fact that only minor concurrent precipitation has occurred during the short annealing time. It may be noted that no cube is yet present, which is found after longer annealing times (cf. Fig. 4b). The texture of C1-2 on the other hand is characterized by a medium strength Cube texture component (slightly ND-rotated) together with a very weak P texture component, see Fig.11b. The texture is very similar to the obtained

one seen at longer annealing times (Fig. 7b). The texture of C1-3 is dominated by an even stronger Cube texture component.

Similar analyses have been conducted for the C2 alloy which contains a higher nominal content of Mn. For the as-cast variant C2-0, a grain structure of elongated grains along the RD direction is obtained, as seen in Fig.12a. The average grain size is slightly larger than for its counterpart C1-0, indicating that some more concurrent precipitation may have occurred during this first 5 s of heating time for the C2-0 variant, consistent with the higher Mn content of this alloy. A much coarser grain structure is produced for C2-2 as shown in Fig.12b, mainly reflecting the significant amount of pre-existing fine dispersoids for this material (cf. Table 2). For C2-3 a homogenous and very fine grained structure is obtained. Accelerated nucleation of recrystallization by PSN might have taken place, since a smaller recrystallized grain size is obtained as compared to C1-3. However, PSN is not expected to be strong, supported by the relatively small constituent particle size (average size only slightly large than 1 μm) and weak P texture (see Fig.13c).

The texture of the three variants of the C2 alloy annealed at 500 °C for 5 s are shown in Fig.13. It is interesting to notice that only a weak P-texture component is obtained for the C2-0 condition, while also a distinct ND-rotated cube component shows up after longer annealing times (Cf. Fig. 5d). For C2-2 both components are present already after 5s of annealing. Turning to C2-3 the P and ND-rotated components are replaced by a medium strength (true) cube component. A general increase in texture strength is obtained from the as-cast variant C2-0 to C2-3. For C2-2 and as well as for C2-3, the recrystallization textures do not change with longer annealing times (Fig. 13b and c vs Fig. 7d and Fig. 9d, respectively).

Concurrent precipitation of dispersoids has less effect on recrystallization behaviour during annealing at high temperatures due to fast recrystallization kinetics. The effect is dependent of

the supersaturation level of alloying elements in solids solution. For instance after annealing at 500°C, C1-0 shows a fine but slightly elongated grain structure (Fig. 10a), while the C2-0 shows a structure with more elongated grains (Fig. 12a). Even at high temperatures, the pre-existing dispersoids can still have a strong effect on nucleation of recrystallization. This has been clearly indicated by the different microstructures of C2-2 and C2-3 after annealing at 500°C for 5s, as shown in Fig. 12b and c. The increased electrical conductivity values for both cases are actually weak and similar (~0.7m/Ωmm^2), meaning that the effect of weak concurrent precipitation on recrystallization is similar. So the difference in terms of grain size can be ascribed to the different amount of pre-existing dispersoids, where more pre-existing dispersoids more strongly suppress nucleation of recrystallization and lead to coarser grain structure. The same conclusion can be obtained if we analyse the cases of C1-2 and C2-2. Also here a limited, and alsmost similar increase in electrical conductivity during annealing of the first 5s is observed (~0.6 and 0.7 m/Ωmm2 respectively), while quite different recrystallized microstructures were obtained as shown in Fig.10b and Fig.12b.

4. Conclusions

Microstructural evolution of two Al-Mn-Fe-Si alloys with different amounts of Mn (0.4 and 1.0 wt%, respectively) during annealing after cold rolling has been carried out. The softening behaviour has been monitored by hardness measurements and electrical conductivity, and the final microstructure in terms of grain structure and texture has been characterized by EBSD. The following conclusions can be made based on the results shown in this paper:

1) It is clearly demonstrated that the amount of Mn and the actual microchemistry state as determined by the homogenization procedure strongly influence the softening behaviour where both a fine dispersion of pre-existing dispersoids as well as strong concurrent precipitation may slow down kinetics considerably and affect both recrystallized grain size and texture. The effects were more pronounced in the alloy with higher nominal content of Mn, but they were qualitatively similar, either the precipitates were pre-existing or resulted mainly from concurrent precipitation.

2) Annealing at high temperatures where concurrent precipitation was mainly avoided before onset of recrystallization resulted in a fine-grained recrystallized structure with textures characterized by a medium to strong cube texture component, and weak P texture and ND-rotated cube texture components. The intensity of the cube component increased with decreasing initial solute content of Mn in solid solution. Annealing at lower temperatures lead to coarse and elongated grain structures and textures dominated by the P and ND-rotated cube components with no or limited cube. For some cases the ND-rotations was as large as 35-45^{o}, which indeed are somewhat strange texture components.

3) Both pre-existing dispersoids and concurrent precipitation are found to retard nucleation of recrystallization and affect final recrystallized grain structure even at the highest annealing temperatures where fast recrystallization kinetics is usually observed. The observation that concurrent precipitation also affects nucleation clearly indicates that nucleation is not truly site saturated, but evolves with time. This is an important point with respect to further model developments, where present available models commonly are based on this assumption.

4) Following the observations above, the results also show that the final grain structure and texture is largely determined already at that nucleation stage, where strongly suppressed nucleation also slows down the recrystallization kinetics (fewer grains grow), an effect which

is further enhanced by a significant Zener drag also acting during recrystallization. As far as results are available, the textures do not seem to change significantly during recrystallization.

Acknowledgments

This research work has been supported by the KMB project (193179/I40) in Norway. The financial support by the Research Council of Norway and the industrial partners, Hydro Aluminium and Sapa Technology is gratefully acknowledged. KH acknowledges the financial support from NTNU, through the Strategic Area Materials.

References

[1] F.J. Humphreys, M.Hatherly, Recrystallization and Related Annealing Phenomena, Second ed., Elsevier, Oxford, 2004.

[2] F.J. Humphreys, Acta. Metall. 25(1977) 1323-1344.

[3] R.D. Doherty, D.A. Hughes, F.J. Humphreys, J.J. Jonas, D. Juul Jensen, M.E. Kassner et al, Mater. Sci. Eng. A 238(1997) 219-274.

[4] F.J. Humphreys, Acta. Mater 45(1997) 4231-4240.

[5] F.J. Humphreys, Scr. Mater. 43(2000) 591-596.

[6] O. Daaland, E. Nes, Acta. Mater. 44 (1996) 1413-1435.

[7] Y.H. Zhang, D. Juul Jensen, Y.B. Zhang, F.X. Lin, Z.Q. Zhang, Q. Liu, Scr. Mater. 67 (2012) 320-323.

[8] E. Nes, N. Ryum, O. Hunderi, Acta. Metall. 33(1985) 11-22.

[9] F.J. Humphreys, P.N. Kalu, Acta. Metall. Mater. 35 (1987) 2815-2829.

[10] W.B. Hutchinson, A. Oscarsson, Å. Karlsson, Mater. Sci. Technol. 5 (1989) 1118-1127.

[11] O. Engler, Z. Liu, K. Kuknke, J. Alloys. Compd. 560 (2013) 111-122

[12] O. Egnler, G. Laptyeva, N. Wang, Mater. Charact. 79(2013) 60-75.

[13] Y. Birol, Scr. Mater. 60 (2009) 5-8.

[14] Y. Birol, Mater. Charact. 80 (2013) 69-75.

[15] Y. Totik, M.Gavgali, Mater. Charact. 49 (2002) 261-268.

[16] T. Radetic, M. Popovic, E. Romhanji, Mater. Charact. 65 (2012)16-27.

[17] M. Somerday, F.J. Humphreys, Mater. Sci. Technol. 19 (2003) 20-29.

[18] Q. Du, W.J. Poole, M.A. Wells, N.C. Parson, Acta. Mater. 61 (2013) 4961-4973.

[19] R.D. Doherty, K. Kashyap, S. Panchanadeeswaran, Acta. Metal. Mater. 4 (1993) 3029-3053.

[20] T. Furu, H.R. Shercliff, G.J. Baxter, C.M. Sellars, Acta. Mater. 47 (1999) 2377-2389.

[21] R.A. Vandermeer, D. Juul Jensen. Acta. Mater. 49 (2001) 2083-2094.

[22] X.M. Cheng, J.G. Morris, Mater. Sci. Eng. A 323 (2002) 32-41.

[23] C. Maurice, J.H. Driver, Acta. Metall. Mater. 41 (1993) 1653-1664.

[24] J. Liu, J.G. Morris, Metall. Mater. Trans. A 34 (2003) 2029-2032.

[25] W.C. Liu, J.G. Morris, Metall. Mater. Trans. A 26 (2005) 2829-2848

[26] O. Engler, X.W. Kong, K. Lucke. Acta. Mater. 49 (2001) 1701-1715.

[27] S. Tangen, K. Sjølstad, T. Furu, E. Nes, Metall. Mater. Trans. A 41 (2010) 2970-2983

[28] N. Wang, J.E. Flatøy, Y.J. Li, K. Marthinsen, Trans. Nonferrous. Met. Soc. China. 22 (2012) 1878-1883.

[29] N. Wang, Y.J. Li, K. Marthinsen, Mater. Sci. Forum. 753 (2013) 231-234.

[30] N. Wang, Y.J. Li, K. Marthinsen, To be submitted

[31] N. Wang, Y.J. Li, K. Marthinsen, To be submitted.

[32] E. Hersent, K. Huang, J. Friis, K. Marthinsen, Mater. Sci. Forum. 753 (2013) 143-146.

[33] A.M.F. Muggerud, E.A. Mørtsell, Y.J.Li, R. Holmestad, Mat. Sci. Eng. A 567 (2013) 21-28

[34] K. Huang, Y.J. Li, K. Marthinsen. Submitted to Trans. Nonferrous. Met. Soc. China.

Z.G.Zang, Y.J.Zhang, J. Mod. Opt. 59 (2012) 161-165.

Z.G.Zang, Y.J.Zhang, Appl. Opt. 51(2012) 3424-3430

Table captions

Table 1 Chemical composition of the two AA 3xxx model alloys, in wt %

Table 2 The electrical conductivity, concentrations of solute (wt% Mn), diameter and number density of constituent particles and dispersoids of the different material conditions.

Figure captions

Fig.1 EBSD micrographs of the typical microstructure before back annealing a) As-cast state of C1; b) C1-3 after deformation to $\varepsilon = 3.0$.

Fig.2 Backscatter electron SEM images to show the constituent particles and dispersoids in the as-cast state and two as-homogenized states of C1 and C2. The dispersoids are shown in the insets which are approximately taken from positions indicated by the square frames. a) C1-0; b) C1-2; c) C1-3 d) C2-0; e) C2-2; f) C2-3.

Fig.3 Variation of Vickers hardness of: a) C1-0 and C2-0; b) C1-2 and C2-2; c) C1-3 and C2-3; and electrical conductivity of: d) C1-0 and C2-0; e) C1-2 and C2-2; f) C1-3 and C2-3.

Fig.4 EBSD maps showing the microstructure of C1-0 and C2-0 after annealing at different temperatures for 10^5 s. a) C1-0, T=400^{o}C, d_{Av}=56.5 μm; b) C1-0, T=500^{o}C, d_{Av}=21.0 μm; c) C2-0, T=400^{o}C,d_{Av}=205.5 μm; d) C2-0, T=500^{o}C,d_{Av}=29.7 μm.

Fig.5 ODF maps showing the recrystallization textures of C1-0 and C2-0 after annealing at different temperatures for 10^5 s. a) C1-0, T=400^{o}C; b) C1-0, T=500^{o}C; c) C2-0, T=400^{o}C; d) C2-0, T=500 ^{o}C.

Fig.6 EBSD maps showing the microstructure of C1-2 and C2-2 after annealing at different temperatures for 10^5 s. a) C1-2, T=400^{o}C, d_{Av}=24.2 μm; b) C1-2, T=500^{o}C, d_{Av}=23.4 μm; c) C2-2, T=400^{o}C, d_{Av}=115.2 μm; d) C2-2, T=500^{o}C, d_{Av}=43.9 μm.

Fig.7 ODF maps showing the recrystallization textures of C1-2 and C2-2 after annealing at different temperatures for 10^5s. a) C1-2, T=400^{o}C; b) C1-2, T=500^{o}C; c) C2-2, T=400^{o}C; d) C2-2, T=500^{o}C.

Fig.8 EBSD maps showing the microstructure of C1-3 and C2-3 after annealing at different temperatures for 10^5 s. a) C1-3,T=300 °C, d_{Av}=19.8 μm; b) C1-3,T=400 °C, d_{Av}=15.6 μm; c) C2-3,T=300 °C, d_{Av}=31.0 μm; d) C2-3,T=400 °C, d_{Av}=12.3 μm.

Fig.9 ODF maps showing the textures of C1-3 and C2-3 after annealing at different temperatures for 10^5 s. a) C1-3, T=300°C; b) C1-3,T=400°C; c) C2-3,T=300°C; d) C2-3,T=400°C.

Fig.10 EBSD maps showing the microstructure of the three variants during isothermal heating experiments after cold rolling to 3.0. a) C1-0, T=500°C, t= 5 s, d_{Av}=18.8 μm; b) C1-2, T=500°C, t=5 s, d_{Av}=22.3 μm; c) C1-3,T=500°C, t=5 s, d_{Av}=17.9 μm .

Fig.11 ODF maps showing the textures of the three variants during isothermal heating experiments after cold rolling to 3.0. a) C1-0, T=500°C, t= 5 s; b) C1-2, T=500°C, t=5 s; c) C1-3, T=500°C, t=5 s.

Fig.12 EBSD maps showing the microstructure of the three variants during isothermal heating experiments after cold rolling to 3.0. a) C2-0, T=500 °C, t= 5 s, d_{Av}=25.0 μm; b) C2-2, T=500 °C, t=5 s, d_{Av}=45.2 μm; c) C2-3, T=500 °C, t=5 s, d_{Av}=12.2 μm.

Fig.13 ODF maps showing the textures of the three variants during isothermal heating experiments after cold rolling to 3.0. a) C2-0, T=500 °C, t= 5 s; b) C2-2, T=500 °C, t=5 s; c) C2-3, T=500 °C, t=5 s.

Table 1
Chemical composition of the two AA 3xxx model alloys, in wt %.

Alloy	Si	Fe	Mn	Others
C1	0.152	0.530	0.390	< 0.01
C2	0.152	0.530	0.970	< 0.01

Table 2
The electrical conductivity, concentrations of solute (wt% Mn), diameter and number density of constituent particles and dispersoids of the different material conditions.

	Electrical conductivity ($m/\Omega mm^2$)	Concentration of Mn (wt%)	Constituent particles		Dispersoids	
			Diameter (μm)	Number density (mm^{-2})	Diameter (μm)	Number density (mm^{-2})
C1-0	23.9	0.35	0.88	2.8e4	–	–
C1-2	27.5	0.16	0.96	2.9e4	0.054	1.3e6
C1-3	29.0	0.11	1.10	2.1e4	0.127	5.5e4
C2-0	17.6	0.69	0.8	3.3e4	–	–
C2-2	23.4	0.23	1.0	2.3e4	0.105	2.8e6
C2-3	23.6	0.21	1.5	1.3e4	0.156	0.9e6

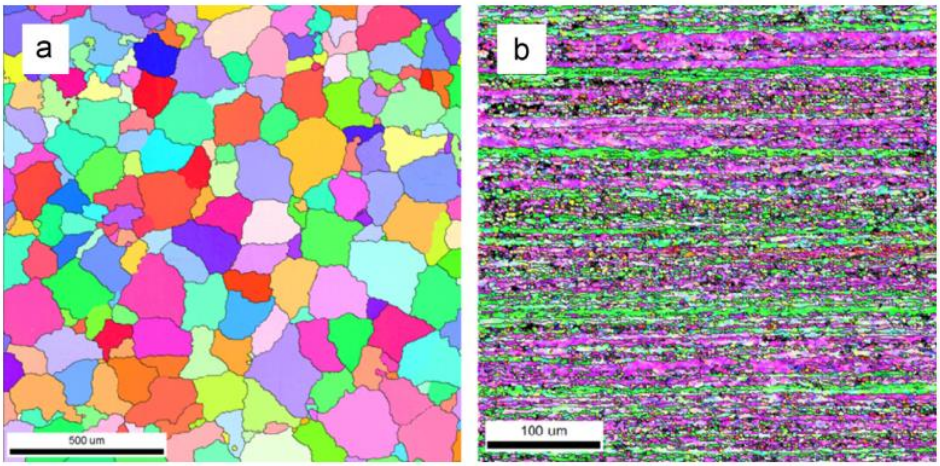

Fig. 1. EBSD micrographs of the typical microstructure before back annealing (a) As-cast state of C1; (b) C1-3 after deformation to $\varepsilon = 3.0$.

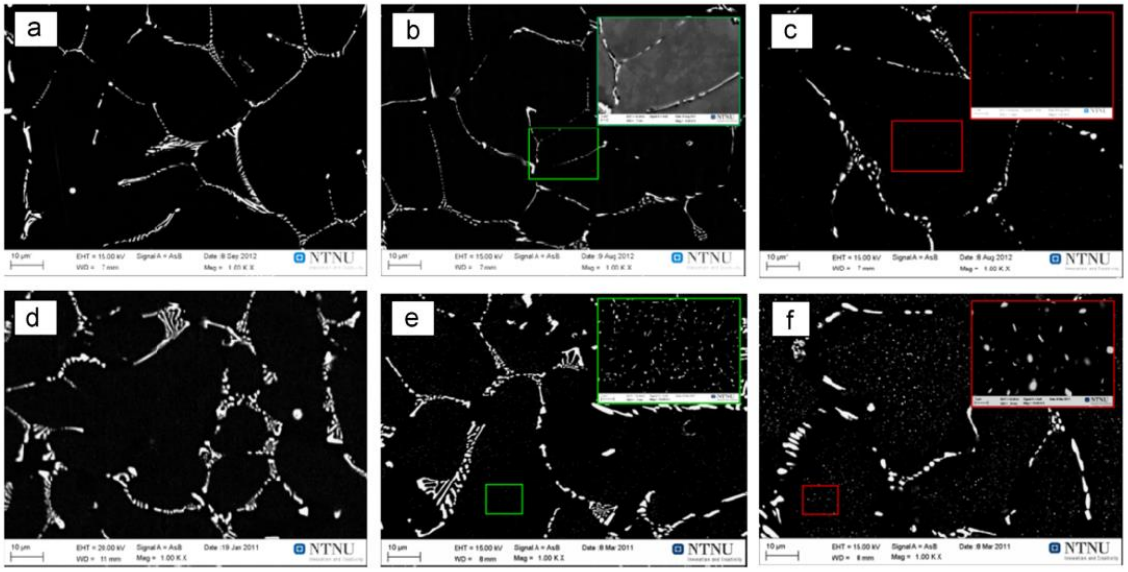

Fig. 2. Backscatter electron SEM images to show the constituent particles and dispersoids in the as-cast state and two as-homogenized states of C1 and C2. The dispersoids are shown in the insets which are approximately taken from positions indicated by the square frames. (a) C1-0; (b) C1-2; (c) C1-3; (d) C2-0; (e) C2-2; (f) C2-3.

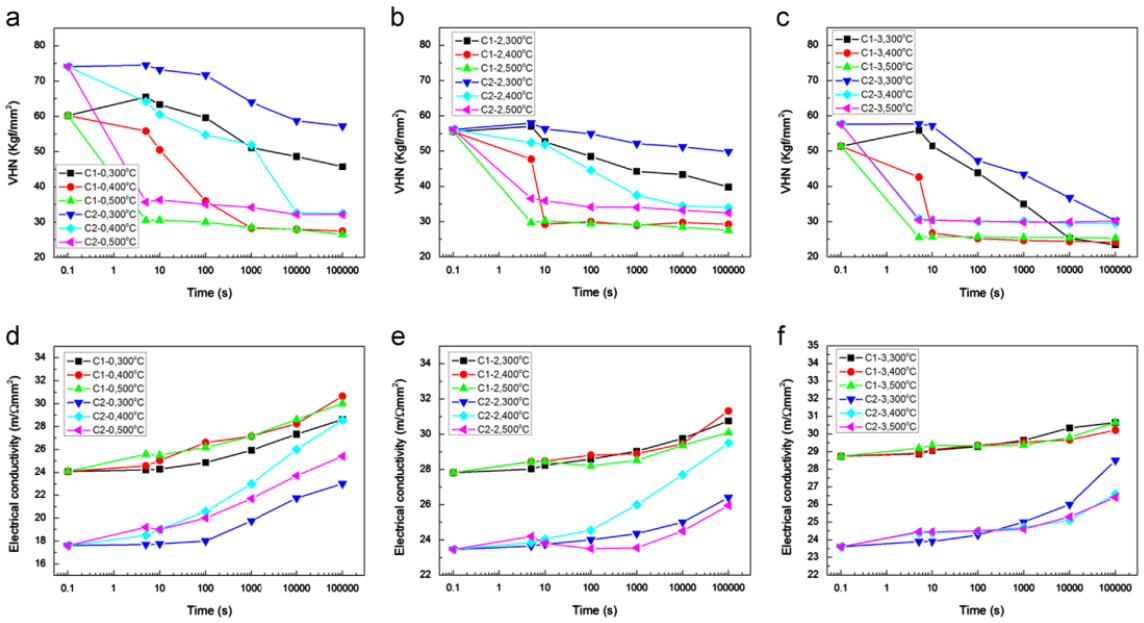

Fig. 3. Variation of Vickers hardness of: (a) C1-0 and C2-0; (b) C1-2 and C2-2; (c) C1-3 and C2-3; and electrical conductivity of: (d) C1-0 and C2-0; (e) C1-2 and C2-2; (f) C1-3 and C2-3.

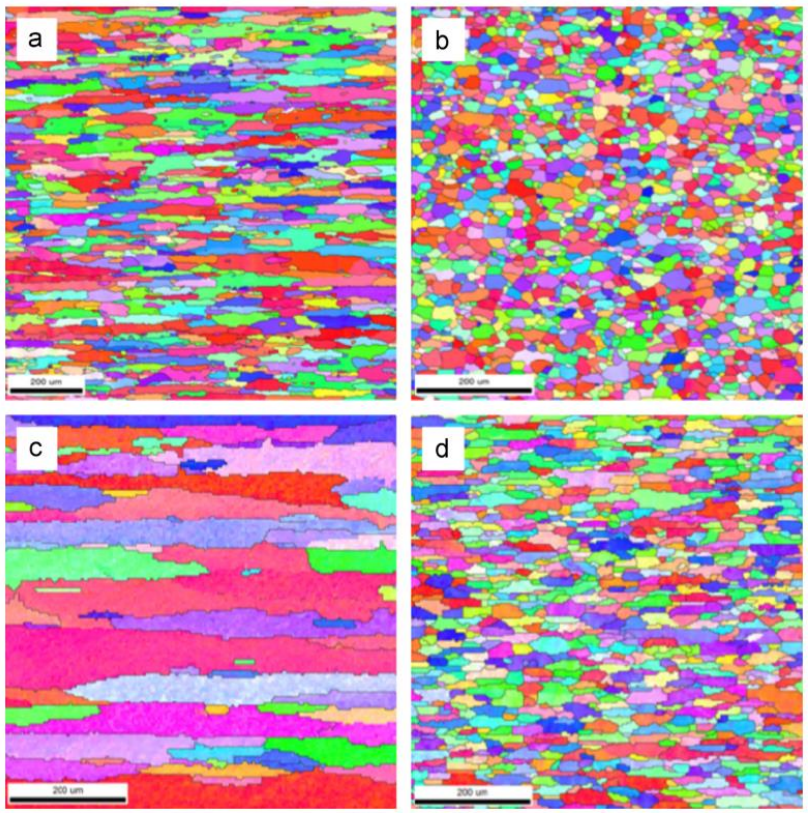

Fig. 4. EBSD maps showing the microstructure of C1-0 and C2-0 after annealing at different temperatures for 10^5 s. (a) C1-0, T=400 °C, d_{Av}=56.5 μm; (b) C1-0, T=500 °C, d_{Av}=21.0 μm; (c) C2-0, T=400 °C, d_{Av}=205.5 μm; (d) C2-0, T=500 °C, d_{Av}=29.7 μm.

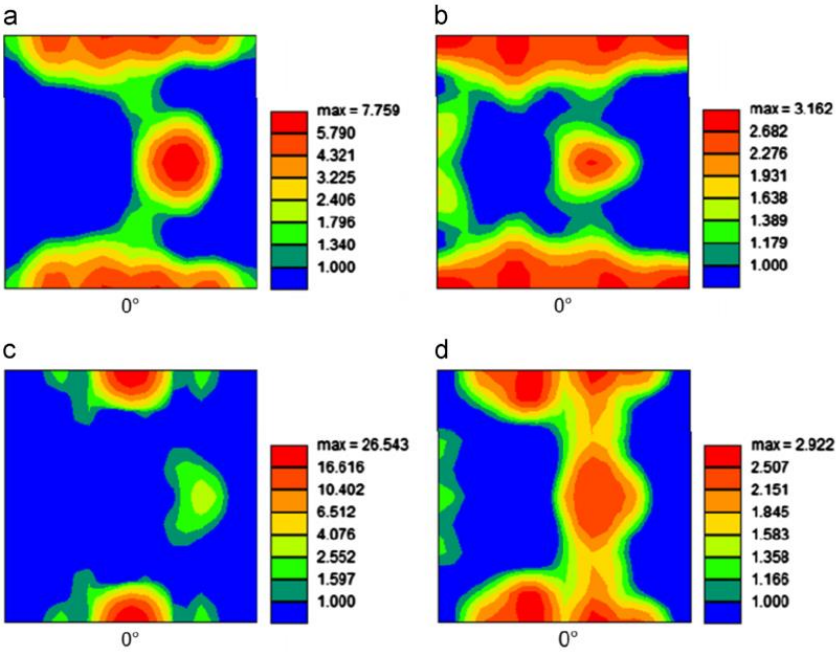

Fig. 5. ODF maps showing the recrystallization textures of C1-0 and C2-0 after annealing at different temperatures for 10^5 s. (a) C1-0, T=400 °C; (b) C1-0, T=500 °C; (c) C2-0, T=400 °C; (d) C2-0, T=500 °C.

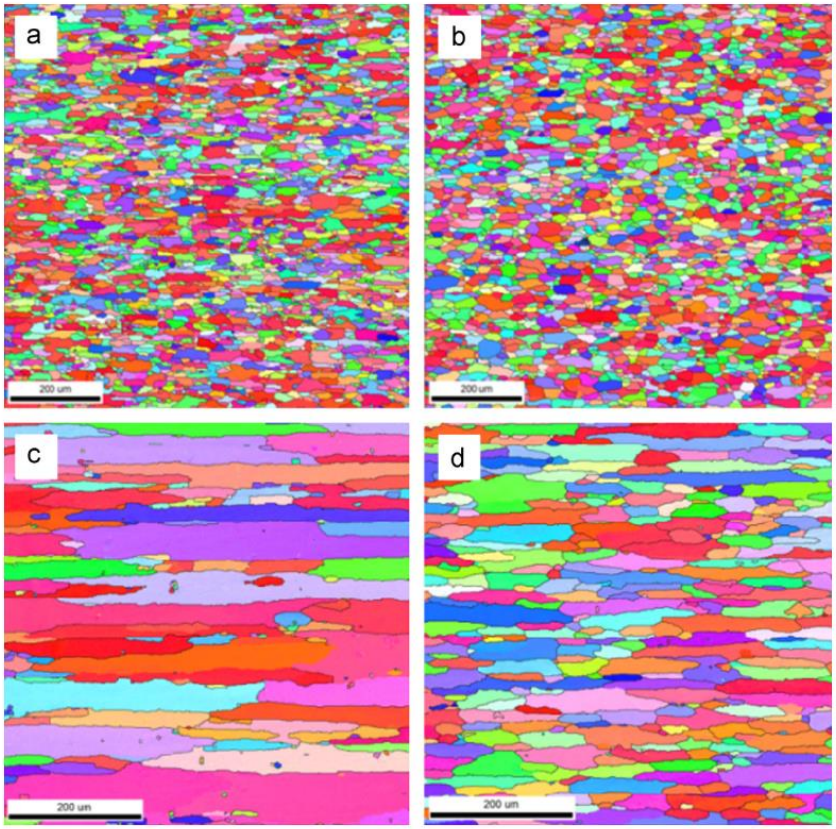

Fig. 6. EBSD maps showing the microstructure of C1-2 and C2-2 after annealing at different temperatures for 10^5 s. (a) C1-2, T=400 °C, d_{Av}=24.2 μm; (b) C1-2, T=500 °C, d_{Av}=23.4 μm; (c) C2-2, T=400 °C, d_{Av}=115.2 μm; (d) C2-2, T=500 °C, d_{Av}=43.9 μm.

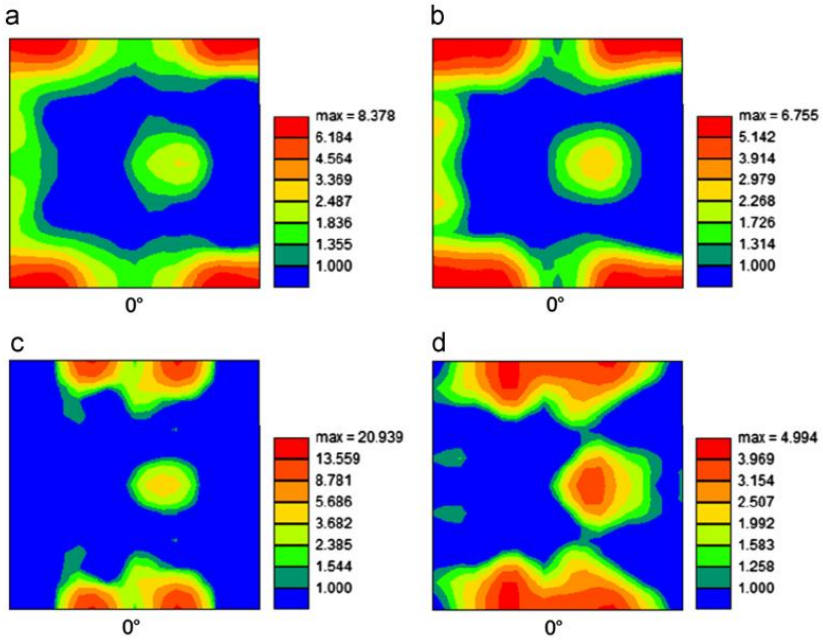

Fig. 7. ODF maps showing the recrystallization textures of C1-2 and C2-2 after annealing at different temperatures for 10^5 s. (a) C1-2, T=400 °C; (b) C1-2, T=500 °C; (c) C2-2, T=400 °C; (d) C2-2, T=500 °C.

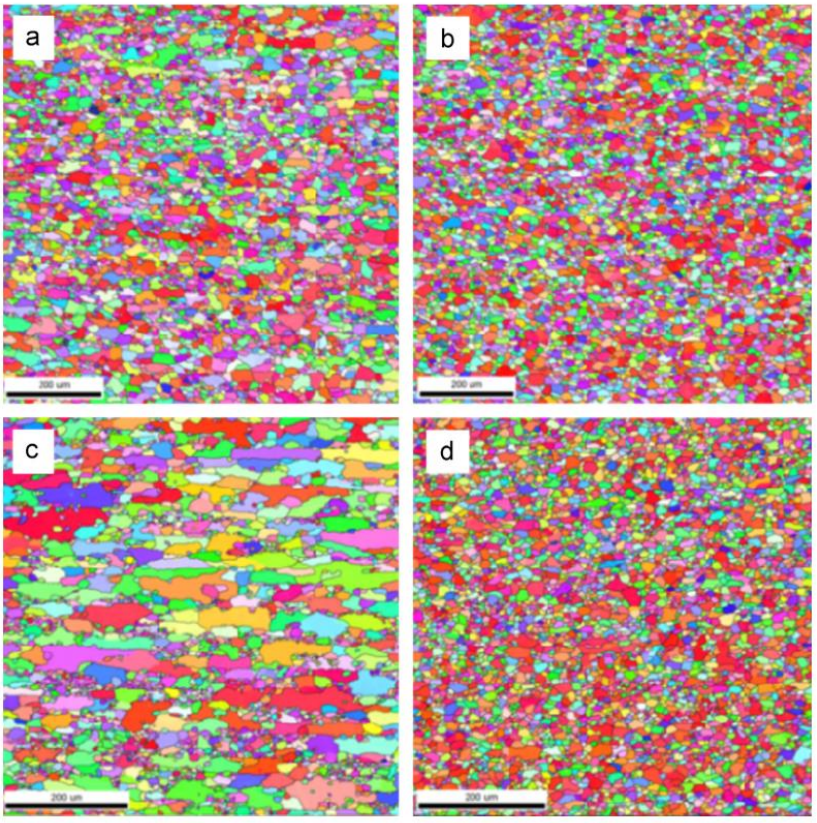

Fig. 8. EBSD maps showing the microstructure of C1-3 and C2-3 after annealing at different temperatures for 10^5 s. (a) C1-3, T=300 °C, d_{Av}=19.8 μm; (b) C1-3, T=400 °C, d_{Av}=15.6 μm; (c) C2-3, T=300 °C, d_{Av}=31.0 μm; (d) C2-3, T=400 °C, d_{Av}=12.3 μm.

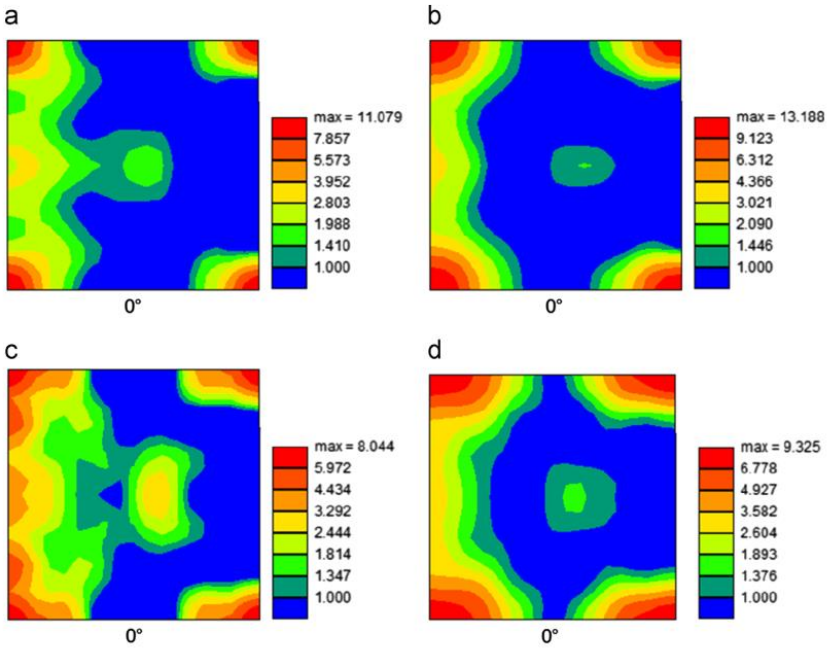

Fig. 9. ODF maps showing the textures of C1-3 and C2-3 after annealing at different temperatures for 10^5 s. (a) C1-3, T=300 °C; (b) C1-3, T=400 °C; (c) C2-3, T=300 °C; (d) C2-3, T=400 °C.

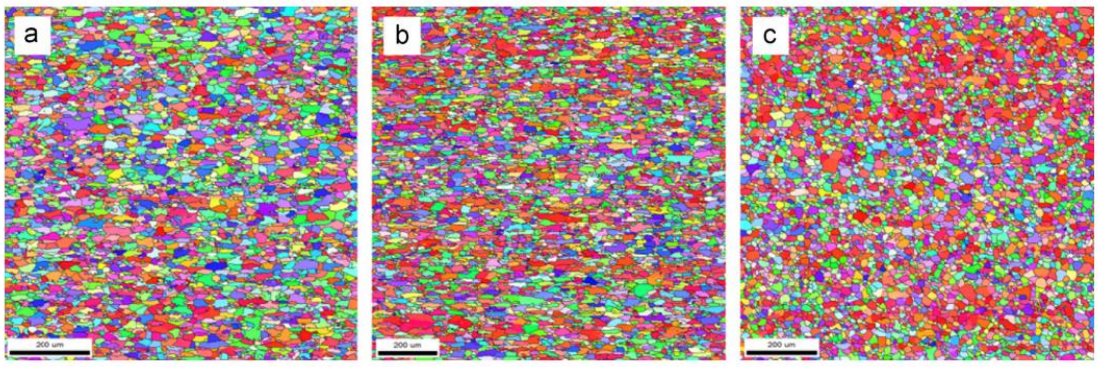

Fig. 10. EBSD maps showing the microstructure of the three variants during isothermal heating experiments after cold rolling to 3.0. (a) C1-0, T=500 °C, t=5 s, d_{Av}=18.8 μm; (b) C1-2, T=500 °C, t=5 s, d_{Av}=22.3 μm; (c) C1-3, T=500 °C, t=5 s, d_{Av}=17.9 μm.

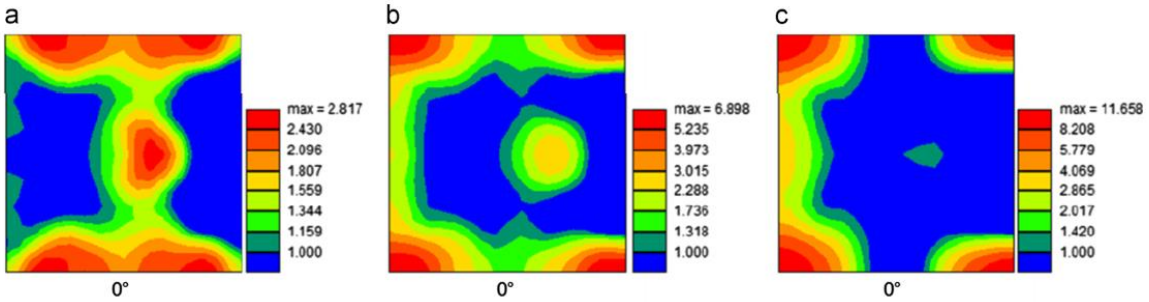

Fig. 11. ODF maps showing the textures of the three variants during isothermal heating experiments after cold rolling to 3.0. (a) C1-0, T=500 °C, t=5 s; (b) C1-2, T=500 °C, t=5 s; (c) C1-3, T=500 °C, t=5 s.

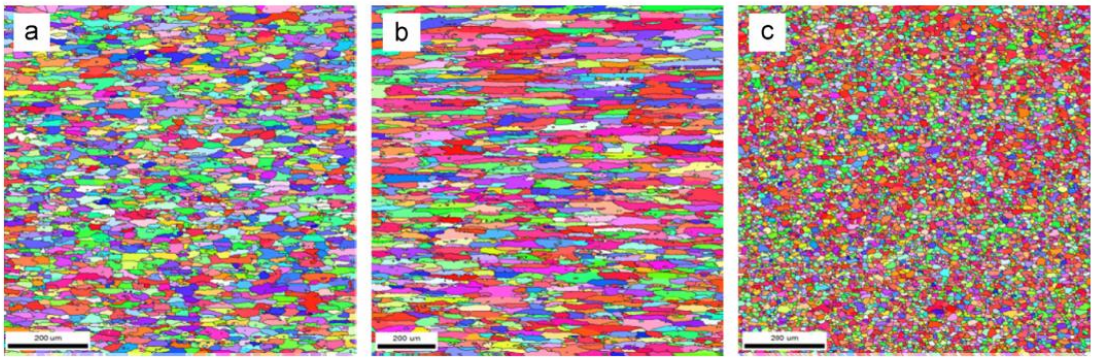

Fig. 12. EBSD maps showing the microstructure of the three variants during isothermal heating experiments after cold rolling to 3.0. (a) C2-0, T=500 °C, t=5 s, d_{Av}=25.0 μm; (b) C2-2, T=500 °C, t=5 s, d_{Av}=45.2 μm; (c) C2-3, T=500 °C, t=5 s, d_{Av}=12.2 μm.

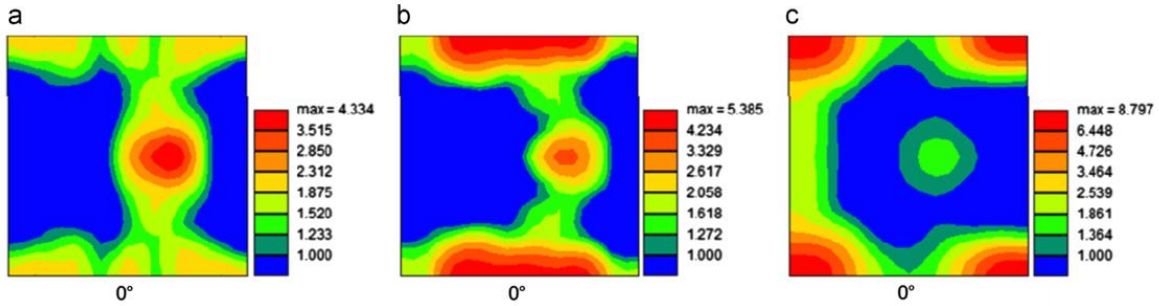

Fig. 13. ODF maps showing the textures of the three variants during isothermal heating experiments after cold rolling to 3.0. (a) C2-0, T=500 °C, t=5 s; (b) C2-2, T=500 °C, t=5 s; (c) C2-3, T=500 °C, t=5 s.